Chapter 7

Kerr-Lens and Additive Pulse Mode Locking

There are many ways to generate saturable absorber action. One can use real saturable absorbers, such as semiconductors or dyes and solid-state laser media. One can also exploit artificial saturable absorbers. The two most prominent artificial saturable absorber modelocking techniques are called Kerr-Lens Mode Locking (KLM) and Additive Pulse Mode Locking (APM). APM is sometimes also called Coupled-Cavity Mode Locking (CCM). KLM was invented in the early 90's [1][2][3][4][5][6][7], but was already predicted to occur much earlier [8][9][10].

7.1 Kerr-Lens Mode Locking (KLM)

The general principle behind Kerr-Lens Mode Locking is sketched in Fig. 7.1. A pulse that builds up in a laser cavity containing a gain medium and a Kerr medium experiences not only self-phase modulation but also self focussing, that is nonlinear lensing of the laser beam, due to the nonlinear refractive index of the Kerr medium. A spatio-temporal laser pulse propagating through the Kerr medium has a time dependent mode size as higher intensities acquire stronger focussing. If a hard aperture is placed at the right position in the cavity, it strips of the wings of the pulse, leading to a shortening of the pulse. Such combined mechanism has the same effect as a saturable absorber. If the electronic Kerr effect with response time of a few femtoseconds or less is used, a fast saturable absorber has been created. Instead of a sep-
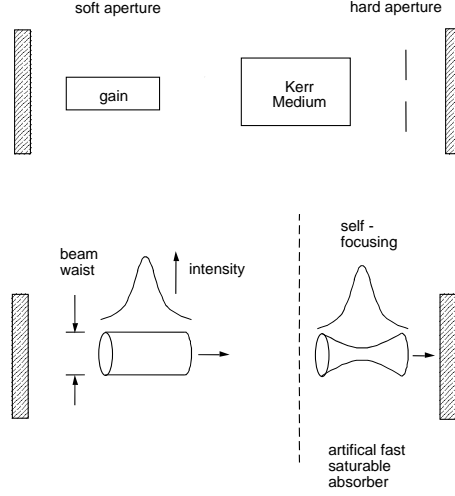
Figure 7.1: Principle mechanism of KLM. The hard aperture can be also replaced by the soft aperture due to the spatial variation of the gain in the laser crystal.

arate Kerr medium and a hard aperture, the gain medium can act both as a Kerr medium and as a soft aperture (i.e. increased gain instead of saturable absorption). The sensitivity of the laser mode size on additional nonlinear lensing is drastically enhanced if the cavity is operated close to the stability boundary of the cavity. Therefore, it is of prime importance to understand the stability ranges of laser resonators. Laser resonators are best understood in terms of paraxial optics [11][12][14][13][15].

7.1.1 Review of Paraxial Optics and Laser Resonator Design

The solutions to the paraxial wave equation, which keep their form during propagation, are the Hermite-Gaussian beams. Since we consider only the fundamental transverse modes, we are dealing with the Gaussian beam

$$U(r, z) = \frac{U_o}{q(z)} \exp\left[-jk\frac{r^2}{2q(z)}\right], \tag{7.1}$$

with the complex q-parameter $q = a + jb$ or its inverse

$$\frac{1}{q(z)} = \frac{1}{R(z)} - j\frac{\lambda}{\pi w^2(z)}. \tag{7.2}$$

The Gaussian beam intensity $I(z,r) = |U(r,z)|^2$ expressed in terms of the power P carried by the beam is given by

$$I(r,z) = \frac{2P}{\pi w^2(z)} \exp\left[-\frac{2r^2}{w^2(z)}\right]. \tag{7.3}$$

The use of the q-parameter simplifies the description of Gaussian beam propagation. In free space propagation from z_1 to z_2, the variation of the beam parameter q is simply governed by

$$q_2 = q_1 + z_2 - z_1, \tag{7.4}$$

where q_2 and q_1 are the beam parameters at z_1 and z_2. If the beam waist, at which the beam has a minimum spot size w_0 and a planar wavefront $(R = \infty)$, is located at $z = 0$, the variations of the beam spot size and the radius of curvature are explicitly expressed as

$$w(z) = w_o \left[1 + \left(\frac{\lambda z}{\pi w_o^2}\right)^2\right]^{1/2}, \tag{7.5}$$

and

$$R(z) = z \left[1 + \left(\frac{\pi w_o^2}{\lambda z}\right)^2\right]. \tag{7.6}$$

The angular divergence of the beam is inversely proportional to the beam waist. In the far field, the half angle divergence is given by,

$$\theta = \frac{\lambda}{\pi w_o}, \tag{7.7}$$
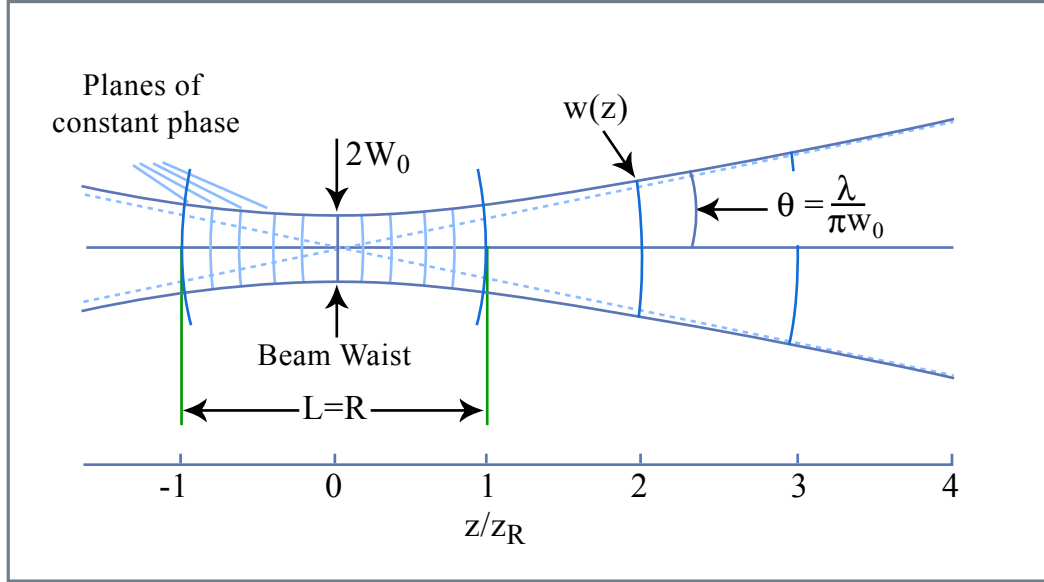
as illustrated in Figure 7.2.

Figure 7.2: Gaussian beam and its characteristics.

Figure by MIT OCW.

Due to diffraction, the smaller the spot size at the beam waist, the larger the divergence. The Rayleigh range is defined as the distance from the waist over which the beam area doubles and can be expressed as

$$z_R = \frac{\pi w_o^2}{\lambda}. \tag{7.8}$$

The confocal parameter of the Gaussian beam is defined as twice the Rayleigh range

$$b = 2z_R = \frac{2\pi w_o^2}{\lambda}, \tag{7.9}$$

and corresponds to the length over which the beam is focused. The propagation of Hermite-Gaussian beams through paraxial optical systems can be efficiently evaluated using the ABCD-law [11]

$$q_2 = \frac{Aq_1 + B}{Cq_1 + D} \tag{7.10}$$

where q_1 and q_2 are the beam parameters at the input and the output planes of the optical system or component. The ABCD matrices of some optical elements are summarized in Table 7.1. If a Gaussian beam with a waist w_{01} is focused by a thin lens a distance z_1 away from the waist, there will be a

new focus at a distance

$$z_2 = f + \frac{(z_1 - f)f^2}{(z_1 - f)^2 + \left(\frac{\pi w_{01}^2}{\lambda}\right)^2},$$ (7.11)

and a waist w_{02}

$$\frac{1}{w_{02}^2} = \frac{1}{w_{01}^2}\left(1 - \frac{z_1}{f}\right)^2 + \frac{1}{f^2}\left(\frac{\pi w_{01}}{\lambda}\right)^2$$ (7.12)
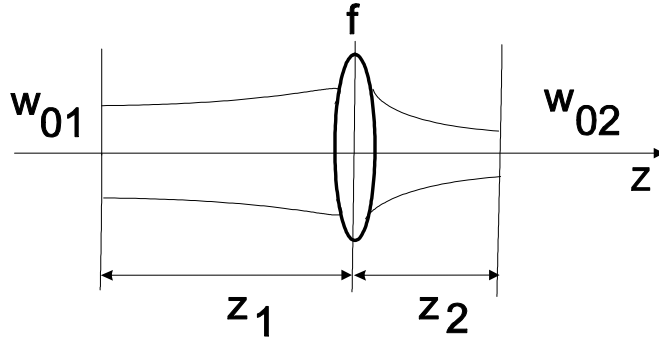

Figure 7.3: Focusing of a Gaussian beam by a lens.

7.1.2   Two-Mirror Resonators

We consider the two mirror resonator shown in Figure 7.4.

Optical Element	ABCD-Matrix
Free Space Distance L	$\begin{pmatrix} 1 & L \\ 0 & 1 \end{pmatrix}$
Thin Lens with focal length f	$\begin{pmatrix} 1 & 0 \\ -1/f & 1 \end{pmatrix}$
Mirror under Angle θ to Axis and Radius R Sagittal Plane	$\begin{pmatrix} 1 & 0 \\ \frac{-2\cos\theta}{R} & 1 \end{pmatrix}$
Mirror under Angle θ to Axis and Radius R Tangential Plane	$\begin{pmatrix} 1 & 0 \\ \frac{-2}{R\cos\theta} & 1 \end{pmatrix}$
Brewster Plate under Angle θ to Axis and Thickness d, Sagittal Plane	$\begin{pmatrix} 1 & \frac{d}{n} \\ 0 & 1 \end{pmatrix}$
Brewster Plate under Angle θ to Axis and Thickness d, Tangential Plane	$\begin{pmatrix} 1 & \frac{d}{n^3} \\ 0 & 1 \end{pmatrix}$

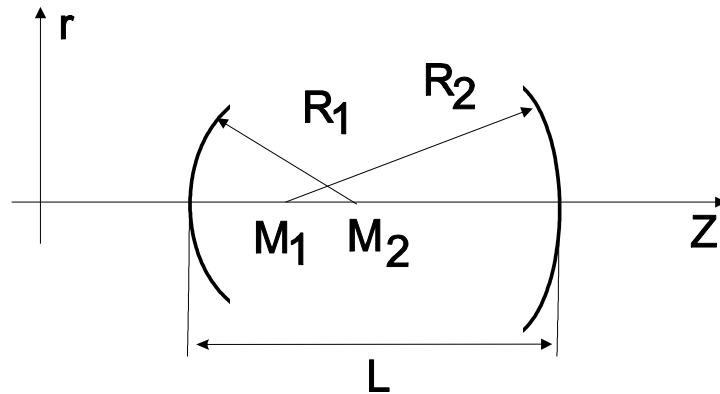Table 7.1: ABCD matrices for commonly used optical elements.

Figure 7.4: Two-Mirror Resonator with curved mirrors with radii of curvature R_1 and R_2.

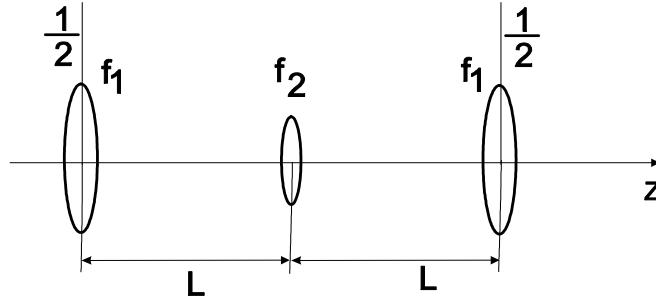The resonator can be unfolded for an ABCD-matrix analysis, see Figure 7.5.

Figure 7.5: Two-mirror resonator unfolded. Note, only one half of the focusing strength of mirror 1 belongs to a fundamental period describing one resonator roundtrip.

The product of ABCD matrices describing one roundtrip according to Figure 7.5 are then given by

$$M = \begin{pmatrix} 1 & 0 \\ \frac{-1}{2f_1} & 1 \end{pmatrix} \begin{pmatrix} 1 & L \\ 0 & 1 \end{pmatrix} \begin{pmatrix} 1 & 0 \\ \frac{-1}{f_2} & 1 \end{pmatrix} \begin{pmatrix} 1 & L \\ 0 & 1 \end{pmatrix} \begin{pmatrix} 1 & 0 \\ \frac{-1}{2f_1} & 1 \end{pmatrix} \quad (7.13)$$

where $f_1 = R_1/2$, and $f_2 = R_2/2$. To carry out this product and to formulate the cavity stability criteria, it is convenient to use the cavity parameters $g_i = 1 - L/R_i, i = 1, 2$. The resulting cavity roundtrip ABCD-matrix can be written in the form

$$M = \begin{pmatrix} (2g_1g_2 - 1) & 2g_2L \\ 2g_1 (g_1g_2 - 1)/L & (2g_1g_2 - 1) \end{pmatrix} = \begin{pmatrix} A & B \\ C & D \end{pmatrix}. \quad (7.14)$$

Resonator Stability

The ABCD matrices describe the dynamics of rays propagating inside the resonator. An optical ray is characterized by the vector $\mathbf{r} = \begin{pmatrix} r \\ r' \end{pmatrix}$, where r is the distance from the optical axis and r' the slope of the ray to the optical axis. The resonator is stable if no ray escapes after many round-trips, which is the case when the eigenvalues of the matrix M are less than one. Since we have a lossless resonator, i.e. $\det|M| = 1$, the product of the eigenvalues has to be 1 and, therefore, the stable resonator corresponds to the case of a complex conjugate pair of eigenvalues with a magnitude of 1. The eigenvalue

equation to M is given by

$$\det|M - \lambda \cdot 1| = \det \left| \begin{pmatrix} (2g_1g_2 - 1) - \lambda & 2g_2L \\ 2g_1(g_1g_2 - 1)/L & (2g_1g_2 - 1) - \lambda \end{pmatrix} \right| = 0, \quad (7.15)$$

$$\lambda^2 - 2(2g_1g_2 - 1)\lambda + 1 = 0. \quad (7.16)$$

The eigenvalues are

$$\lambda_{1/2} = (2g_1g_2 - 1) \pm \sqrt{(2g_1g_2 - 1)^2 - 1}, \quad (7.17)$$

$$= \begin{cases} \exp(\pm\theta), \cosh\theta = 2g_1g_2 - 1, & \text{for } |2g_1g_2 - 1| > 1 \\ \exp(\pm j\psi), \cos\psi = 2g_1g_2 - 1, & \text{for } |2g_1g_2 - 1| \leq 1 \end{cases} . (7.18)$$

The case of a complex conjugate pair with a unit magnitude corresponds to a stable resontor. Therfore, the stability criterion for a stable two mirror resontor is

$$|2g_1g_2 - 1| \leq 1. \quad (7.19)$$

The stable and unstable parameter ranges are given by

$$\text{stable} \quad : \quad 0 \leq g_1 \cdot g_2 = S \leq 1 \quad (7.20)$$
$$\text{unstable} \quad : \quad g_1g_2 \leq 0; \text{ or } g_1g_2 \geq 1. \quad (7.21)$$

where $S = g_1 \cdot g_2$, is the stability parameter of the cavity. The stability criterion can be easily interpreted geometrically. Of importance are the distances between the mirror mid-points M$_i$ and cavity end points, i.e. $g_i = (R_i - L)/R_i = -S_i/R_i$, as shown in Figure 7.6.
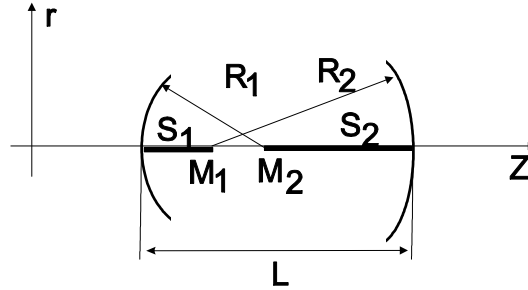

Figure 7.6: The stability criterion involves distances between the mirror mid-points M$_i$ and cavity end points. i.e. $g_i = (R_i - L)/R_i = -S_i/R_i$.

The following rules for a stable resonator can be derived from Figure 7.6 using the stability criterion expressed in terms of the distances S_i. Note, that the distances and radii can be positive and negative

$$\text{stable} : 0 \leq \frac{S_1 S_2}{R_1 R_2} \leq 1. \tag{7.22}$$

The rules are:

- A resonator is stable, if the mirror radii, laid out along the optical axis, overlap.

- A resonator is unstable, if the radii do not overlap or one lies within the other.

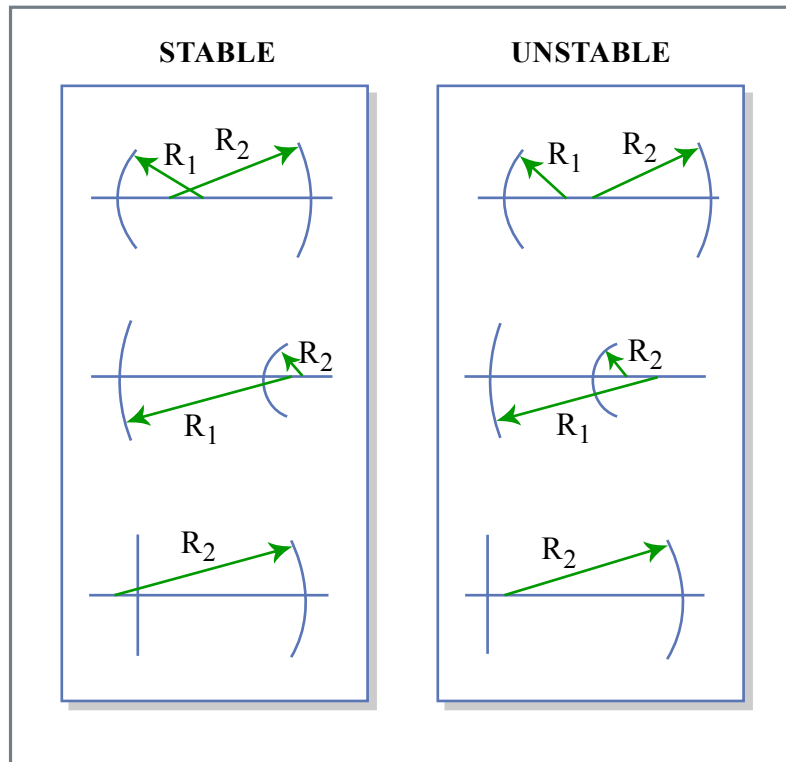Figure 7.7 shows stable and unstable resonator configurations.

Figure 7.7: Illustration of stable and unstable resonator configurations.

Figure by MIT OCW.

For a two-mirror resonator with concave mirrors and $R_1 \leq R_2$, we obtain the general stability diagram as shown in Figure 7.8. There are two ranges for the mirror distance L, within which the cavity is stable, $0 \leq L \leq R_1$ and
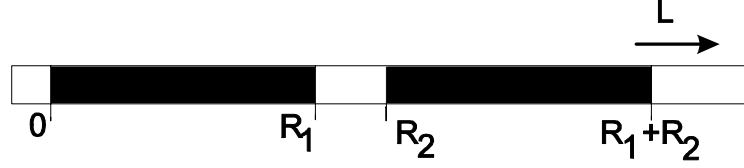
Figure 7.8: Stabile regions (black) for the two-mirror resonator.

$R_2 \leq L \leq R_1 + R_2$. It is interesting to investigate the spot size at the mirrors and the minimum spot size in the cavity as a function of the mirror distance L.

Resonator Mode Characteristics

The stable modes of the resonator reproduce themselves after one round-trip, i.e. from Eq.(7.10) we find

$$q_1 = \frac{Aq_1 + B}{Cq_1 + D} \tag{7.23}$$

The inverse q-parameter, which is directly related to the phase front curvature and the spot size of the beam, is determined by

$$\left(\frac{1}{q}\right)^2 + \frac{A - D}{B}\left(\frac{1}{q}\right) + \frac{1 - AD}{B^2} = 0. \tag{7.24}$$

The solution is

$$\left(\frac{1}{q}\right)_{1/2} = -\frac{A - D}{2B} \pm \frac{j}{2|B|}\sqrt{(A + D)^2 - 1} \tag{7.25}$$

If we apply this formula to (7.15), we find the spot size on mirror 1

$$\left(\frac{1}{q}\right)_{1/2} = -\frac{j}{2|B|}\sqrt{(A + D)^2 - 1} = -j\frac{\lambda}{\pi w_1^2}. \tag{7.26}$$

or

$$\begin{aligned}
w_1^4 &= \left(\frac{2\lambda L}{\pi}\right)^2 \frac{g_2}{g_1}\frac{1}{1 - g_1 g_2} \tag{7.27} \\
&= \left(\frac{\lambda R_1}{\pi}\right)^2 \frac{R_2 - L}{R_1 - L}\left(\frac{L}{R_1 + R_2 - L}\right). \tag{7.28}
\end{aligned}$$

By symmetry, we find the spot size on mirror 3 via switching index 1 and 2:

$$w_2^4 = \left(\frac{2\lambda L}{\pi}\right)^2 \frac{g_1}{g_2}\frac{1}{1-g_1g_2} \tag{7.29}$$

$$= \left(\frac{\lambda R_2}{\pi}\right)^2 \frac{R_1 - L}{R_2 - L}\left(\frac{L}{R_1 + R_2 - L}\right). \tag{7.30}$$

The intracavity focus can be found by transforming the focused Gaussian beam with the propagation matrix

$$M = \begin{pmatrix} 1 & z_1 \\ 0 & 1 \end{pmatrix}\begin{pmatrix} 1 & 0 \\ \frac{-1}{2f_1} & 1 \end{pmatrix}$$

$$= \begin{pmatrix} 1 - \frac{z_1}{2f_1} & z_1 \\ \frac{-1}{2f_1} & 1 \end{pmatrix}, \tag{7.31}$$

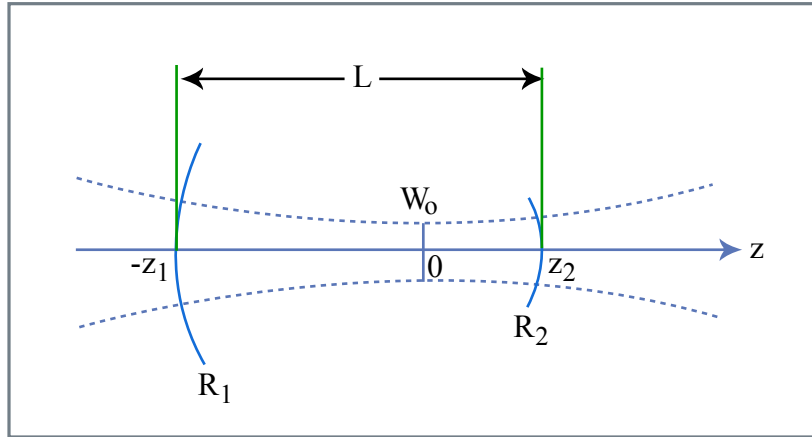to its new focus by properly choosing z_1, see Figure 7.9.

Figure 7.9: Two-mirror resonator

Figure by MIT OCW.

A short calculation results in

$$z_1 = L\frac{g_2(g_1 - 1)}{2g_1g_2 - g_1 - g_2} \tag{7.32}$$

$$= \frac{L(L - R_2)}{2L - R_1 - R_2}, \tag{7.33}$$

and, again, by symmetry

$$z_2 = L\frac{g_1(g_2 - 1)}{2g_1g_2 - g_1 - g_2} \tag{7.34}$$

$$= \frac{L(L - R_1)}{2L - R_1 - R_2} = L - z_1. \tag{7.35}$$

The spot size in the intracavity focus is

$$
\begin{aligned}
w_o^4 &= \left(\frac{\lambda L}{\pi}\right)^2 \frac{g_1 g_2 \left(1 - g_1 g_2\right)}{(2g_1 g_2 - g_1 - g_2)^2} & (7.36) \\
&= \left(\frac{\lambda}{\pi}\right)^2 \frac{L(R_1 - L)(R_2 - L)(R_1 + R_2 - L)}{(R_1 + R_2 - 2L)^2}. & (7.37)
\end{aligned}
$$

All these quantities for the two-mirror resonator are shown in Figure 7.11. Note, that all resonators and the Gaussian beam are related to the confocal resonator as shown in Figure 7.10.

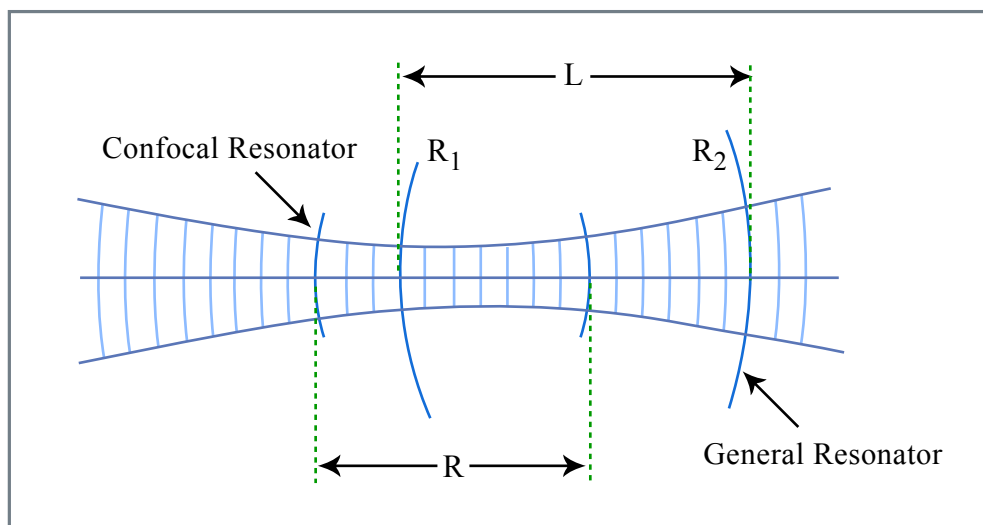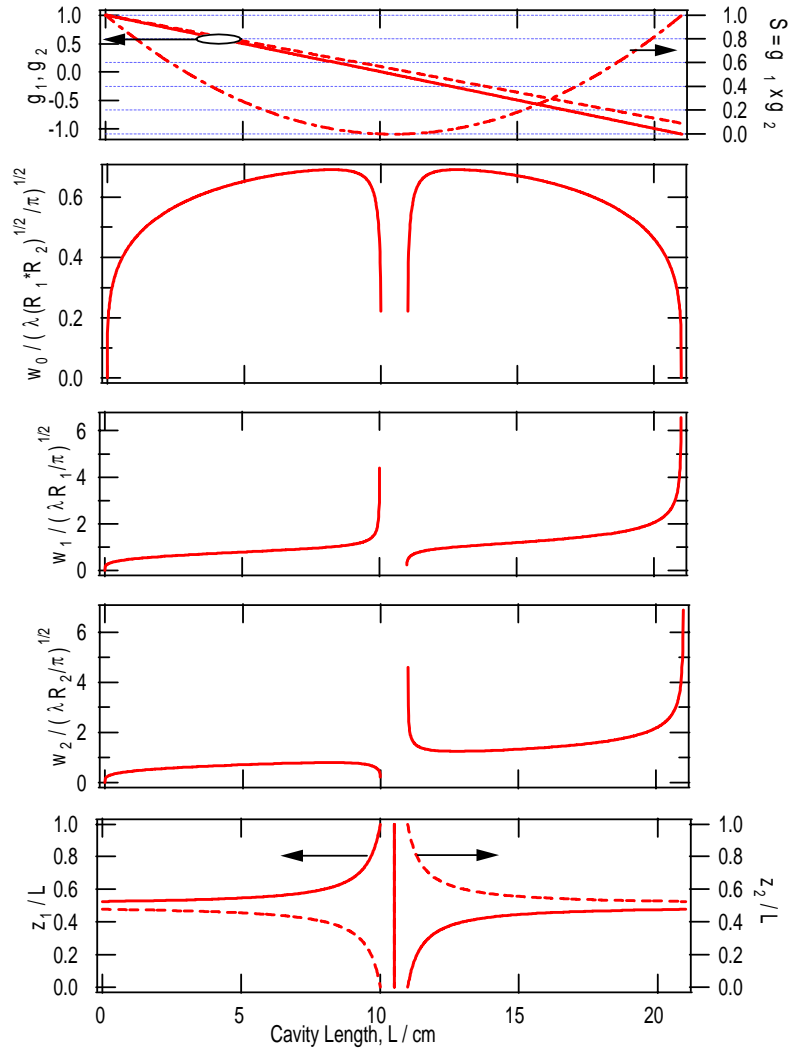Figure 7.10: Two-mirror resonator and its relationship with the confocal resonator.

Figure 7.11: From top to bottom: Cavity parameters, g_1, g_2, S, w_0, w_1, w_2, z_1 and z_2 for the two-mirror resonator with $R_1 = 10$ cm and $R_2 = 11$ cm.

7.1.3 Four-Mirror Resonators

More complex resonators, like the four-mirror resonator depicted in Figure 7.12 a) can be transformed to an equivalent two-mirror resonator as shown in Figure 7.4 b) and c)
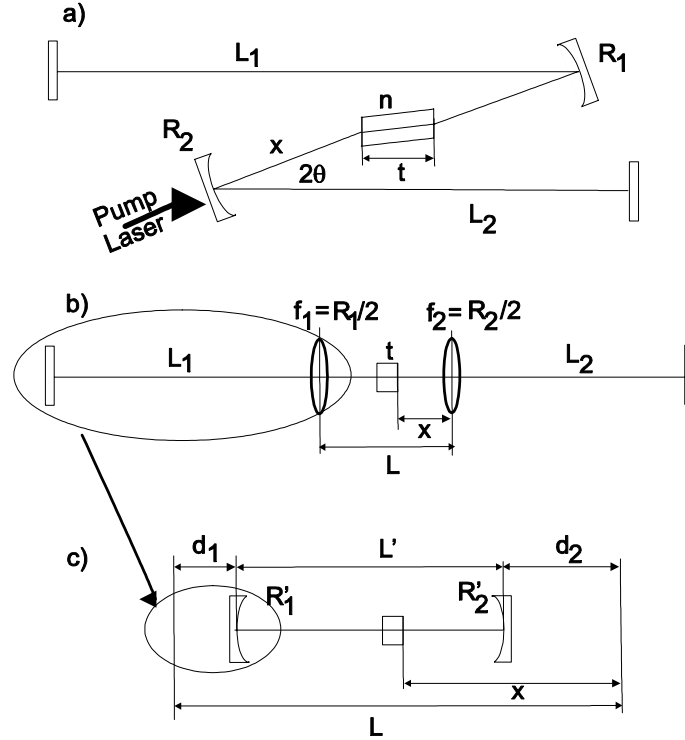

Figure 7.12: a) Four-mirror resonator with gain medium of refractive index n, and thickness t. Folding angles have to be adjusted for astigmatism compensation. b) Equivalent lens cavity. Note that the new focal length do not yet account for the different equivalent radii of curvature due to nonnormal incidence on the mirrors. c) Equivalent two-mirror cavity with imaged end mirrors.

Each of the resonator arms (end mirror,L_1, R_1) or (end mirror, L_2, R_2) is equivalent to a new mirror with a new radius of curvature $R'_{1/2}$ positioned a distance $d_{1/2}$ away from the old reference plane [12]. This follows simply from the fact that each symmetric optical system is equivalent to a lens positioned

at a distance d from the old reference plane

$$
\begin{aligned}
M &= \left(\begin{array}{cc} A & B \\ C & A \end{array} \right) = \left(\begin{array}{cc} 1 & d \\ 0 & 1 \end{array} \right) \left(\begin{array}{cc} 1 & 0 \\ \frac{-1}{f} & 1 \end{array} \right) \left(\begin{array}{cc} 1 & d \\ 0 & 1 \end{array} \right) \\
&= \left(\begin{array}{cc} 1 - \frac{d}{f} & d\left(2 - \frac{d}{f}\right) \\ \frac{-1}{f} & 1 - \frac{d}{f} \end{array} \right)
\end{aligned}
\tag{7.38}
$$

with

$$
d = \frac{A-1}{C}
\tag{7.39}
$$

$$
\frac{-1}{f} = C
$$

The matrix of the resonator arm 1 is given by

$$
M = \left(\begin{array}{cc} 1 & 0 \\ \frac{-2}{R_1} & 1 \end{array} \right) \left(\begin{array}{cc} 1 & 2L_1 \\ 0 & 1 \end{array} \right) \left(\begin{array}{cc} 1 & 0 \\ \frac{-2}{R_1} & 1 \end{array} \right) = \left(\begin{array}{cc} 1 - \frac{4L_1}{R_1} & 2L_1 \\ \frac{-4}{R_1}\left(1 - \frac{2L_1}{R_1}\right) & 1 - \frac{4L_1}{R_1} \end{array} \right)
\tag{7.40}
$$

from which we obtain

$$
d_1 = -\frac{R_1}{2}\frac{1}{1 - R_1/(2L_1)},
\tag{7.41}
$$

$$
R_1' = -\left(\frac{R_1}{2}\right)^2 \frac{1}{L_1\left[1 - R_1/(2L_1)\right]}.
\tag{7.42}
$$

For arm lengths $L_{1/2}$ much larger than the radius of curvature, the new radius of curvature is roughly by a factor of $\frac{R_1}{4L_1}$ smaller. Typical values are $R_1 = 10$ cm and $L_1 = 50$ cm. Then the new radius of curvature is $R_1' = 5$ mm. The analogous equations apply to the other resonator arm

$$
d_2 = -\frac{R_2}{2}\frac{1}{1 - R_2/(2L_2)},
\tag{7.43}
$$

$$
R_2' = -\left(\frac{R_2}{2}\right)^2 \frac{1}{L_2\left[1 - R_2/(2L_2)\right]}.
\tag{7.44}
$$

Note that the new mirror radii are negative for $R_i/L_i < 1$. The new distance L' between the equivalent mirrors is then also negative over the region where the resonator is stable, see Fig.7.8. We obtain

$$
L' = L + d_1 + d_2 = L - \frac{R_1 + R_2}{2} - \delta
\tag{7.45}
$$

$$\delta \;=\; \frac{R_1}{2}\left[\frac{1}{1-R_1/(2L_1)}-1\right]+\frac{R_2}{2}\left[\frac{1}{1-R_2/(2L_2)}-1\right] \qquad (7.46)$$

$$=\; -(R_1'+R_2') \qquad (7.47)$$

or

$$L = \frac{R_1+R_2}{2} - (R_1'+R_2') + L' \qquad (7.48)$$

From the discussion in section 7.1.2, we see that the stability ranges cover at most a distance δ. Figure 7.13 shows the resonator characteristics as a function of the cavity length L for the following parameters $R_1 = R_2 = 10$ cm and $L_1 = 100$ cm and $L_2 = 75$ cm, which lead to

$$\begin{aligned} d_1 &= -5.26 \text{ cm} \\ R_1' &= -0.26 \text{ cm} \end{aligned} , \qquad (7.49)$$

$$\begin{aligned} d_2 &= -5.36 \text{ cm} \\ R_2' &= -0.36 \text{ cm} \end{aligned} , \qquad (7.50)$$

$$L' = L - 10.62 \text{ cm} \qquad (7.51)$$

Note, that the formulas (7.27) to (7.37) can be used with all quantities replaced by the corresponding primed quantities in Eq.(7.49) - (7.51). The result is shown in Fig. 7.13. The transformation from L to L' transforms the stability ranges according to Fig. 7.14. The confocal parameter of the laser mode is approximately equal to the stability range.

Astigmatism Compensation

So far, we have considered the curved mirrors under normal incidence. In a real cavity this is not the case and one has to analyze the cavity performance for the tangential and sagittal beam separately. The gain medium, usually a thin plate with a refractive index n and a thickness t, generates astigmatism. Astigmatism means that the beam foci for sagittal and tangential plane are not at the same position. Also, the stablity regions of the cavity are different for the different planes and the output beam is elliptical. This is so, because a beam entering a plate under an angle refracts differently in both planes, as described by different ABCD matricies for tangential and sagittal plane, see Table 7.1.Fortunately, one can balance the astigmatism of the beam due to
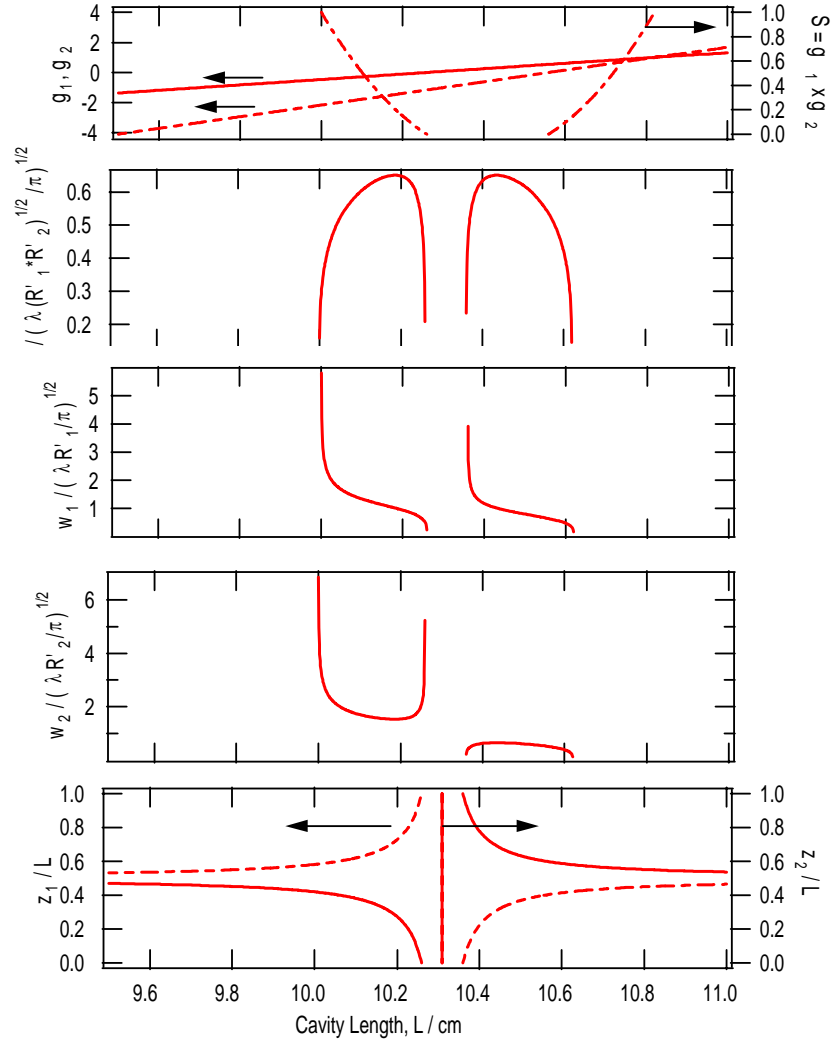
Figure 7.13: From top to bottom: Cavity parameters, g_1, g_2, S, w_0, w_1, w_2, z_1 and z_2 for the four-mirror resonator with $R_1 = R_2 = 10$ cm, $L_1 = 100$ cm and $L_2 = 75$ cm.
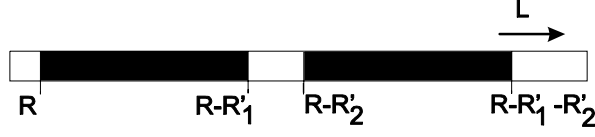
Figure 7.14: Transformed stability range for the four mirror resonator with $R = (R_1 + R_2)/2$.

the plate by the astigmatism introduced by the curved mirrors at a specific incidence angle θ on the mirrors [12]. The focal length of the curved mirrors under an angle are given by

$$
\begin{aligned}
f_s &= f/\cos\theta \\
f_t &= f \cdot \cos\theta
\end{aligned}
\tag{7.52}
$$

The propagation distance in a plate with thickness t under Brewster's angle is given by $t\sqrt{n^2+1}/n$. Thus, the equivalent traversing distances in the sagittal and the tangential planes are (Table 7.1),

$$
\begin{aligned}
d_s &= t\sqrt{n^2+1}/n^2 \\
d_f &= t\sqrt{n^2+1}/n^4
\end{aligned}
\tag{7.53}
$$

The different distances have to compensate for the different focal lengths in the sagittal and tangential planes. Assuming two idential mirrors $R = R_1 = R_2$, leads to the condition

$$
d_s - 2f_s = d_t - 2f_t.
\tag{7.54}
$$

With $f = R/2$ we find

$$
R\sin\theta\tan\theta = Nt, \text{ where } N = \sqrt{n^2+1}\frac{n^2-1}{n^4}
\tag{7.55}
$$

Note, that t is the thickness of the plate as opposed to the path length of the beam in the plate. The equation gives a quadratic equation for $\cos\theta$

$$
\cos^2\theta + \frac{Nt}{R}\cos\theta - 1 = 0
\tag{7.56}
$$

$$\cos \theta_{1/2} = -\frac{Nt}{2R} \pm \sqrt{1 + \left(\frac{Nt}{2R}\right)^2} \qquad (7.57)$$

Since the angle is positive, the only solution is

$$\theta = \arccos\left[\sqrt{1 + \left(\frac{Nt}{2R}\right)^2} - \frac{Nt}{2R}\right]. \qquad (7.58)$$

This concludes the design and analysis of the linear resonator.

7.1.4 The Kerr Lensing Effects

At high intensities, the refractive index in the gain medium becomes intensity dependent

$$n = n_0 + n_2 I. \qquad (7.59)$$

The Gaussian intensity profile of the beam creates an intensity dependent index profile

$$I(r) = \frac{2P}{\pi w^2} \exp\left[-2(\frac{r}{w})^2\right]. \qquad (7.60)$$

In the center of the beam the index can be appoximated by a parabola

$$n(r) = n_0'\left(1 - \frac{1}{2}\gamma^2 r^2\right), \text{ where} \qquad (7.61)$$

$$n_0' = n_0 + n_2\frac{2P}{\pi w^2}, \gamma = \frac{1}{w^2}\sqrt{\frac{8n_2 P}{n_0'\pi}}. \qquad (7.62)$$

A thin slice of a parabolic index medium is equivalent to a thin lens. If the parabolic index medium has a thickness t, then the ABCD matrix describing the ray propagation through the medium at normal incidence is [16]

$$M_K = \begin{pmatrix} \cos \gamma t & \frac{1}{n_0'\gamma} \sin \gamma t \\ -n_0'\gamma \sin \gamma t & \cos \gamma t \end{pmatrix}. \qquad (7.63)$$

Note that, for small t, we recover the thin lens formula ($t \to 0$, but $n_0'\gamma^2 t = 1/f$ =const.). If the Kerr medium is placed under Brewster's angle, we again have to differentiate between the sagittal and tangential planes. For the

sagittal plane, the beam size entering the medium remains the same, but for the tangential plane, it opens up by a factor n_0'

$$
\begin{aligned}
w_s &= w \\
w_t &= w \cdot n_0'
\end{aligned}
\tag{7.64}
$$

The spotsize propotional to w^2 has to be replaced by $w^2 = w_s w_t$. Therefore, under Brewster angle incidence, the two planes start to interact during propagation as the gamma parameters are coupled together by

$$
\gamma_s = \frac{1}{w_s w_t} \sqrt{\frac{8 n_2 P}{n_0' \pi}}
\tag{7.65}
$$

$$
\gamma_t = \frac{1}{w_s w_t} \sqrt{\frac{8 n_2 P}{n_0' \pi}}
\tag{7.66}
$$

Without proof (see [12]), we obtain the matrices listed in Table 7.2. For low

Optical Element	ABCD-Matrix
Kerr Medium Normal Incidence	$M_K = \begin{pmatrix} \cos \gamma t & \frac{1}{n_0' \gamma} \sin \gamma t \\ -n_0' \gamma \sin \gamma t & \cos \gamma t \end{pmatrix}$
Kerr Medium Sagittal Plane	$M_{Ks} = \begin{pmatrix} \cos \gamma_s t & \frac{1}{n_0' \gamma_s} \sin \gamma_s t \\ -n_0' \gamma_s \sin \gamma_s t & \cos \gamma_s t \end{pmatrix}$
Kerr Medium Tangential Plane	$M_{Kt} = \begin{pmatrix} \cos \gamma_t t & \frac{1}{n_0'^3 \gamma_t} \sin \gamma_t t \\ -n_0'^3 \gamma_t \sin \gamma_t t & \cos \gamma_t t \end{pmatrix}$

Table 7.2: ABCD matrices for Kerr media, modelled with a parabolic index profile $n(r) = n_0' \left(1 - \frac{1}{2} \gamma^2 r^2\right)$.

peak power P, the Kerr lensing effect can be neglected and the matrices in Table 7.2 converge towards those for linear propagation. When the laser is mode-locked, the peak power P rises by many orders of magnitude, roughly the ratio of cavity round-trip time to the final pulse width, assuming a constant pulse energy. For a 100 MHz, 10 fs laser, this is a factor of 10^6. With the help of the matrix formulation of the Kerr effect, one can iteratively find the steady state beam waists in the laser. Starting with the values for the linear cavity, one can obtain a new resonator mode, which gives improved

values for the beam waists by calculating a new cavity round-trip propagation matrix based on a given peak power P. This scheme can be iterated until there is only a negligible change from iteration to iteration. Using such a simulation, one can find the change in beam waist at a certain position in the resonator between cw-operation and mode-locked operation, which can be expressed in terms of the delta parameter

$$\delta_{s,t} = \frac{1}{p} \frac{w_{s,t}(P, z) - w_{s,t}(P = 0, z)}{w_{s,t}(P = 0, z)} \tag{7.67}$$

where p is the ratio between the peak power and the critical power for self-focusing

$$p = P/P_{crit}, \text{ with } P_{crit} = \lambda_L^2 / \left(2\pi n_2 n_0^2\right). \tag{7.68}$$

To gain insight into the sensitivity of a certain cavity configuration for KLM, it is interesting to compute the normalized beam size variations $\delta_{s,t}$ as a function of the most critical cavity parameters. For the four-mirror cavity, the natural parameters to choose are the distance between the crystal and the pump mirror position, x, and the mirror distance L, see Figure 7.12. Figure 7.15 shows such a plot for the following cavity parameters $R_1 = R_2 = 10$ cm, $L_1 = 104$ cm, $L_2 = 86$ cm, $t = 2$ mm, $n = 1.76$ and $P = 200$ kW.
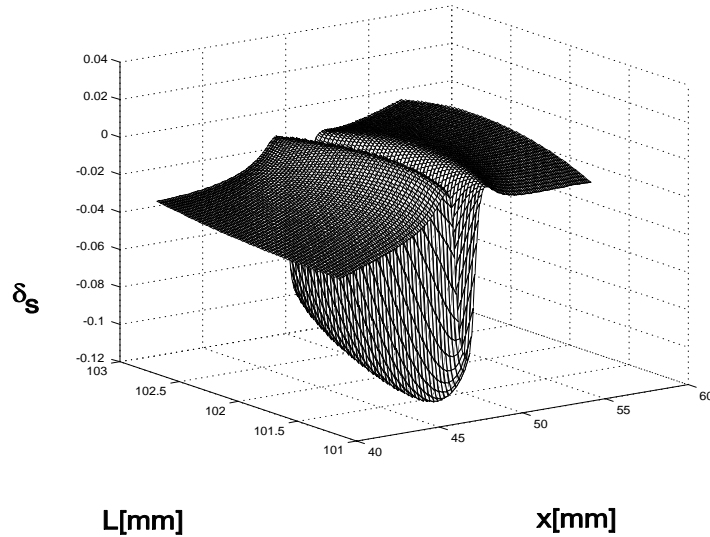

Figure 7.15: Beam narrowing ratio δ_s, for cavity parameters $R_1 = R_2 = 10$ cm, $L_1 = 104$ cm, $L_2 = 86$ cm, $t = 2$ mm, $n = 1.76$ and $P = 200$ kW

The Kerr lensing effect can be exploited in different ways to achieve mode locking.

Soft-Aperture KLM

In the case of soft-aperture KLM, the cavity is tuned in such a way that the Kerr lensing effect leads to a shrinkage of the laser mode when mode-locked. The non-saturated gain in a laser depends on the overlap of the pump mode and the laser mode. From the rate equations for the radial photon distribution $N(r)$ and the inversion $N_P(r)$ of a laser, which are proportional to the intensities of the pump beam and the laser beam, we obtain a gain, that is proportional to the product of $N(r)$ and $N_P(r)$. If we assume that the focus of the laser mode and the pump mode are at the same position and neglect the variation of both beams as a function of distance, we obtain

$$
\begin{aligned}
g \ &\sim \ \int_0^\infty N(r) * N_P(r) r dr \\
&\sim \ \int_0^\infty \frac{2P_P}{\pi w_P^2} \exp\left[-\frac{2r^2}{w_P^2}\right] \frac{2}{\pi w_L^2} \exp\left[-\frac{2r^2}{w_L^2}\right] r dr
\end{aligned}
$$

With the beam cross sections of the pump and the laser beam in the gain medium, $A_P = \pi w_P^2$ and $A_L = \pi w_L^2$,we obtain

$$
g \sim \frac{1}{A_P + A_L}.
$$

If the pump beam is much stronger focused in the gain medium than the laser beam, a shrinkage of the laser mode cross section in the gain medium leads to an increased gain. When the laser operates in steady state, the change in saturated gain would have to be used for the investigation. However, the general argument carries through even for this case. Figure 7.16 shows the variation of the laser mode size in and close to the crystal in a soft-aperture KLM laser due to self-focusing.
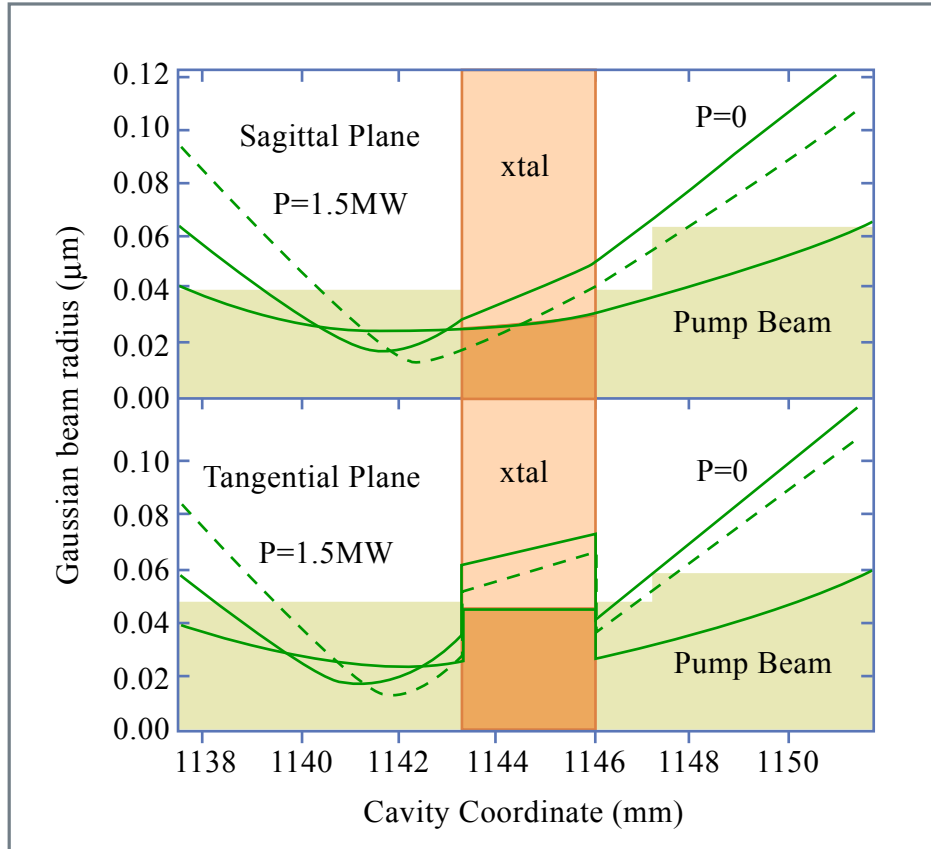
Figure 7.16: Variation of laser mode size in and close to the crystal in a soft aperture KLM laser due to self-focussing.

Figure by MIT OCW.

Hard-Aperture KLM

In a hard-aperture KLM-Laser, one of the resonator arms contains (usually close to the end mirrors) an aperture such that it cuts the beam slightly. When Kerr lensing occurs and leads to a shrinkage of the beam at this position, the losses of the beam are reduced. Note, that depending on whether the aperture is positioned in the long or short arm of the resontor, the operating point of the cavity at which Kerr lensing favours or opposes mode-locking may be quite different (see Figure 7.13).
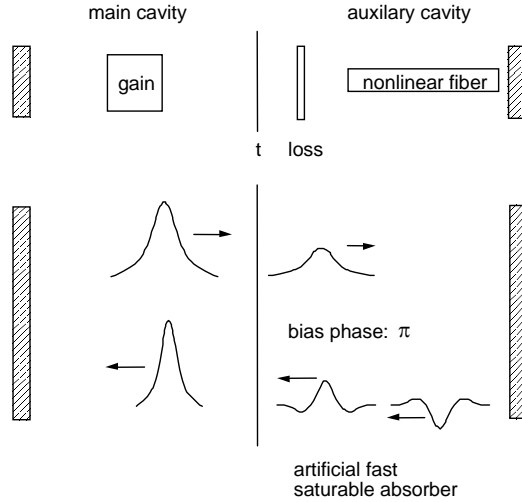
Figure 7.17: Principle mechanism of APM.

7.2   Additive Pulse Mode Locking

Like Kerr-Lens Mode Locking also Additive Pulse Mode Locking (APM) is an artificial saturable absorber effect [17][18][19][20][21][22]. Figure 7.17 shows the general principle at work. A small fraction of the light emitted from the main laser cavity is injected externally into a nonlinear fiber. In the fiber strong SPM occurs and introduces a significant phase shift between the peak and the wings of the pulse. In the case shown the phase shift is π

A part of the modified and heavily distorted pulse is reinjected into the cavity in an interferometrically stable way, such that the injected pulse interferes constructively with the next cavity pulse in the center and destructively in the wings. This superposition leads to a shorter intracavity pulse and the pulse shaping generated by this process is identical to the one obtained from a fast saturable absorber. Again, an artificial saturable absorber action is generated.
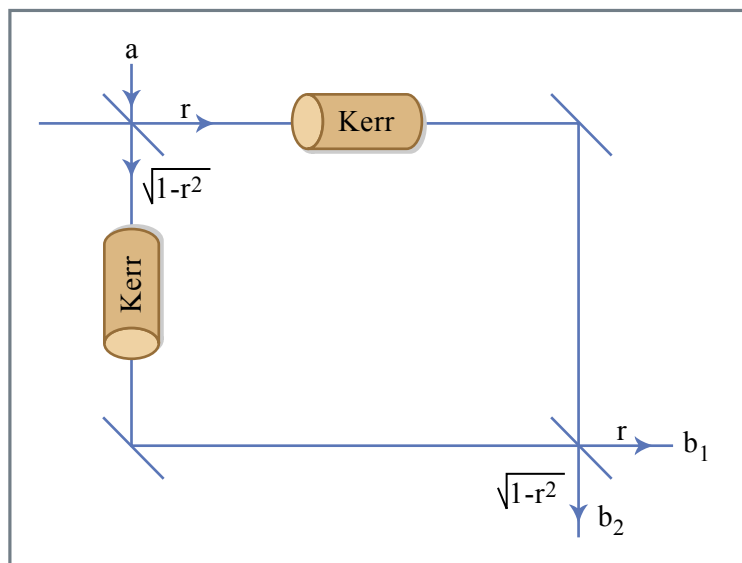
Figure 7.18: Schematic of nonlinear Mach-Zehnder interferometer.

Figure by MIT OCW.

Figure 7.18 shows a simple nonlinear interferometer. In practice, such an interferometer can be realized in a self-stabilized way by the use of both polarizations in an isotropic Kerr medium with polarizer and analyzer as shown in Figure 7.19.
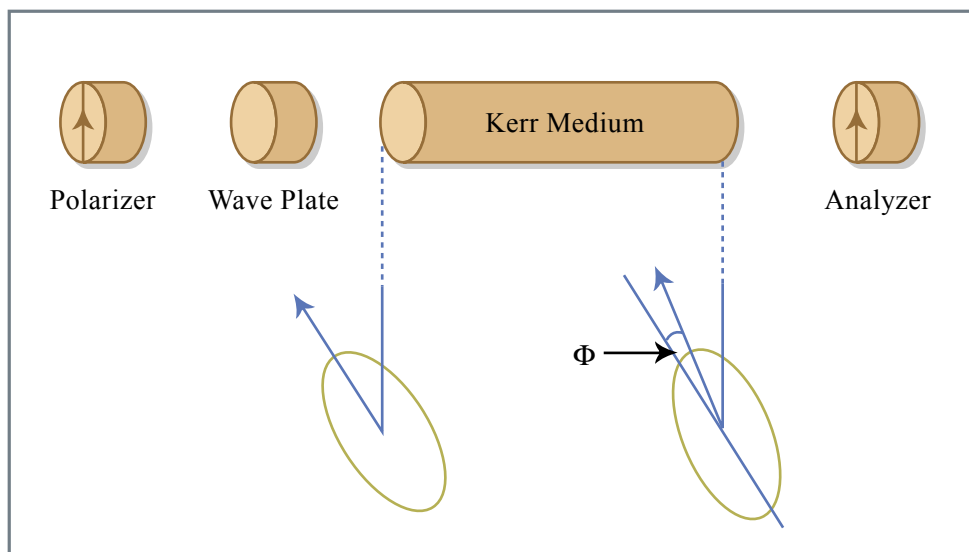

Figure 7.19: Nonlinear Mach-Zehnder interferometer using nonlinear polarization rotation in a fiber [25].

Figure by MIT OCW.

The Kerr effect rotates the polarization ellipse and thus transforms phase modulation into amplitude modulation. The operation is in one-to-one correspondence with that of the nonlinear Mach-Zehnder interferometer of Fig.

7.18. The system of Figure 7.18 can be analyzed rather simply and thus it is worthwhile to look at the derivation and the implicit assumptions. The couplers are described by the scattering matrices

$$S = \begin{bmatrix} r & \sqrt{1-r^2} \\ \sqrt{1-r^2} & -r \end{bmatrix}.$$ (7.69)

The outputs of the interferometer are then

$$b_1 = \left[r^2 e^{-j\phi_1} + (1-r^2)e^{-j\phi_2} \right] a,$$ (7.70)

$$b_2 = 2r\sqrt{1-r^2}\exp\left[-j\frac{\phi_1+\phi_2}{2}\right]\sin\left[\frac{\phi_2-\phi_1}{2}\right] a,$$ (7.71)

ϕ_1 and ϕ_2 are the phase shifts in the two arms composed of both linear "bias" contributions ϕ_{bi} and the Kerr phase shifts ϕ_{Ki}

$$\phi_i = \phi_{bi} + \phi_{Ki}, \; (i = 1, 2),$$ (7.72)

$$\phi_{Ki} = \kappa_i |a|^2, \; (i = 1, 2).$$ (7.73)

The power in output port two is related to the linear and nonlinear losses

$$\begin{aligned} |b_2|^2 &= 2r^2\left(1-r^2\right)\left(1-\cos\left[\phi_2-\phi_1\right]\right)|a|^2 \\ &= 2r^2\left(1-r^2\right)\{(1-\cos\left[\phi_{b2}-\phi_{b1}\right])+ \\ &\quad + \sin\left[\phi_{b2}-\phi_{b1}\right]\left(\phi_{K2}-\phi_{K1}\right)\}|a|^2 \end{aligned}$$ (7.74)

Depending on the bias phase $\phi_b = \phi_{b2} - \phi_{b1}$, the amplitude loss is

$$l = r^2\left(1-r^2\right)\left(1-\cos\phi_b\right)|a|^2,$$ (7.75)

and the $\gamma-$parameter of the equivalent fast saturable absorber is

$$\gamma = \left(\kappa_1 - \kappa_2\right)r^2\left(1-r^2\right)\sin\phi_b.$$ (7.76)

If the interferometer forms part of a resonant system, the frequency of the system is affected by the phase shift of the interferometer and in turn affects the phase.

When the resonant frequencies of the linear system $(\gamma = \delta = 0)$ without the interferometer should remain the resonant frequencies with the interferometer, the net phase shift of the interferometer has to be chosen to be zero. Since a small loss has been assumed and hence $r^2 \gg 1 - r^2$

$$\text{Im}\left[r^2 e^{-j\phi_{b1}} + \left(1-r^2\right)e^{-j\phi_{b2}}\right] = \text{Im}\left[r^2(1-j\phi_{b1}) + \left(1-r^2\right)e^{-j\phi_{b2}}\right] = 0$$ (7.77)

or

$$\phi_{b1} = \frac{-\left(1 - r^2\right)}{r^2} \sin \phi_{b2}. \tag{7.78}$$

and $\cos\phi_{b1} = 1$. With this adjustment, the response of the interferometer becomes

$$\begin{aligned} b_1 &\approx a + \Delta a = a - \left(1 - r^2\right)\left(1 - \cos \phi\right) \ a \\ &\quad -(1 - r^2)\left(\phi_{K2} - \phi_{K1}\right)\sin \phi \ a \\ &\quad -jr^2\phi_{K1} - j(1 - r^2)\phi_{K2}\cos \phi \ a, \end{aligned} \tag{7.79}$$

where we have set $\phi = \phi_{b2}$. This gives for the parameters of the master equation l, γ and δ

$$\begin{aligned} l &= \left(1 - r^2\right)\left(1 - \cos \phi\right), \tag{7.80} \\ \gamma &= \left(\kappa_1 - \kappa_2\right)\left(1 - r^2\right)\sin \phi, \tag{7.81} \\ \delta &= \kappa_1 r^2 + \kappa_2(1 - r^2)\cos \phi. \tag{7.82} \end{aligned}$$

Due to the special choice of the bias phase there is no contribution of the nonlinear interferometer to the linear phase. This agrees with expressions (7.75) and (7.76). The Kerr coefficients are

$$\kappa_1 = r^2 \left(\frac{2\pi}{\lambda}\right)\frac{n_2}{A_{eff}}L_{Kerr}, \tag{7.83}$$

$$\kappa_2 = \left(1 - r^2\right)\left(\frac{2\pi}{\lambda}\right)\frac{n_2}{A_{eff}}L_{Kerr}. \tag{7.84}$$

Here, λ is the free space wavelength of the optical field, A_{eff} is the effective area of the mode, n_2 the intensity dependent refractive index, and L_{Kerr} is the length of the Kerr medium. Figure 7.20 is the saturable absorber coefficient γ normalized to the loss and Kerr effect (note that γ goes to zero when the loss goes to zero) as a function of r^2.
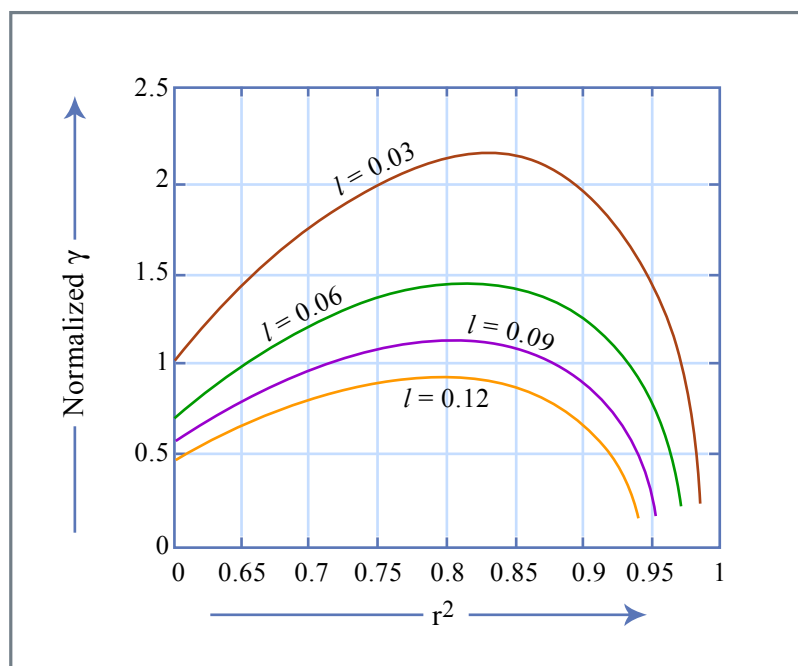
Figure 7.20: Normalized saturable absorber coefficient $\gamma / \left[\left(\frac{2\pi}{\lambda} \right) \frac{n_2}{A_{eff}} L_{Kerr} \; l \right]$ as a function of r^2 with loss l as parameter [25].

Figure by MIT OCW.

Large saturable absorber coefficients can be achieved at moderate loss values.

Bibliography

[1] D. E. Spence, P. N. Kean, W. Sibbett, "60-fsec pulse generation from a self-mode-locked Ti:Sapphire laser", Opt. Lett. **16**, pp. 42 – 44 (1991)

[2] U. Keller, G. W 'tHooft, W. H. Knox, J. E. Cunningham, "Femtosecond Pulses from a Continuously Self-Starting Passively Mode-Locked Ti:Sapphire Laser," Opt. Lett. **16**, pp.1022 – 1024 (1991).

[3] D. K. Negus, L. Spinelli, N. Goldblatt, G. Feugnet, "Sub-100 femtosecond pulse generation by Kerr lens modelocking in Ti:Sapphire," in Advanced Solid-State Lasers, G. Dube, L. Chase, Eds. (Optical Society of America, Washington, D.C., 1991), **10**, pp.120 – 124.

[4] F. Salin, J. Squier and M. Piche, "Mode locking of $Ti:Al_2O_3$ lasers and self-focusing: a Gaussian approximation," Opt. Lett. **16**, pp. 1674 – 1676 (1991).

[5] M. Piche, F. Salin, "Self-mode locking of solid-state lasers without apertures", Opt. Lett. **18**, pp. 1041 – 1043 (1993).

[6] G. Cerullo, S. De Silvestri, V. Magni, L. Pallaro, "Resonators for Kerr-lens mode-locked femtosecond Ti:sapphire lasers", Opt. Lett. **19**, pp. 807 – 809 (1994).

[7] G. Cerullo, S. De Silvestri, V. Magni, "Self-starting Kerr Lens Mode-Locking of a Ti:Sapphire Laser", Opt. Lett. **19**, pp. 1040 – 1042 (1994).

[8] L. Dahlström, "Passive modelocking and Q-switching of high power lasers by means of the optical Kerr effect," Opt. Comm. **5**, pp. 157 – 162 (1972).

[9] E. G. Lariontsev and V. N. Serkin, "Possibility of using self-focusing for increasing contrast and narrowing of ultrashort light pulses," Sov. J. Quant. Electron. **5**, pp. 769 – 800 (1975).

[10] K. Sala, M. C. Richardson, N. R. Isenor, "Passive modelocking of Lasers with the optical Kerr effect modulator," IEEE J. Quant. Electron. QE-13, pp. 915 – 924 (1977).

[11] H. Kogelnik and T. Li, "Laser Beams and Resonators," Appl. Opt. **5**, pp. 1550 – 1566 (1966).

[12] H. Kogelnik, E. P. Ippen, A. Dienes and C. V. Shank, "Astigmatically Compensated Cavities for CW Dye Lasers," IEEE J. Quantum Electron. **QE-8**, pp. 373 – 379 (1972).

[13] O. Svelto, "Principles of Lasers," 3rd Edition, Plenum Press, New York and London, (1989).

[14] H. A. Haus, "Fields and Waves in Optoelectronics", Prentice Hall 1984.

[15] F. K. Kneubühl and M. W. Sigrist, "Laser," 3rd Edition, Teubner Verlag, Stuttgart (1991).

[16] A. E. Siegman, "Lasers," University Science Books, Mill Valley, California (1986).

[17] K. J. Blow and D. Wood, "Modelocked lasers with nonlinear external cavities," J. Opt. Soc. Am. B **5**, pp. 629 – 632 (1988).

[18] K. J. Blow and B. P. Nelson, "Improved mode locking of an F-center laser with a nonlinear nonsoliton external cavity," Opt. Lett. **13**, pp. 1026 –1028 (1988).

[19] P. N. Kean, X. Zhu, D. W. Crust, R. S. Grant, N. Langford and W. Sibbett, "Enhanced mode locking of color-center lasers," Opt. Lett. **14**, pp. 39 – 41 (1989).

[20] J. Mark, L. Y. Liu, K. L. Hall, H. A. Haus and E. P. Ippen, "Femtosecond pulse generation in a laser with a nonlinear external resonator," Opt. Lett. **14**, pp. 48 – 50 (1989).

[21] E. P. Ippen, H. A. Haus and L. Y. Liu, "Additive pulse mode locking," J. Opt. Soc. Am. B **6**, pp. 1736 – 1745 (1989).

[22] J. Goodberlet, J. Jacobson and J. G. Fujimoto, P. A. Schultz and T. Y. Fan, "Self-starting additive-pulse mode-locked diode-pumped Nd:YAG laser", Opt. Lett. **15**, pp. 504 –506 (1990).

[23] F. X. Kärtner, L. R. Brovelli, D. Kopf, M. Kamp, I. Calasso and U. Keller: "Control of Solid-State Laser Dynamics by Semiconductor Devices, Optical Engineering, **34**, pp. 2024 – 2036, (1995).

[24] K. Tamura, "Additive-pulse limiting", Opt. Lett. **19**, pp. 31 – 33 (1994).

[25] H. A. Haus, J. G. Fujimoto and E. P. Ippen, "Analytic Theory of Additive Pulse and Kerr Lens Mode Locking," IEEE J. Quantum Electron. **28**, pp. 2086 – 2095 (1992).

[26] H. A. Haus, J. G. Fujimoto and E. P. Ippen, "Structures of Additive Pulse Mode Locking," J. Opt. Soc. Am. **8**, pp. 2068 – 2076 (1991).